arXiv:1006.4506v1 [cond-mat.supr-con] 23 Jun 2010

Giant anharmonicity suppresses superconductivity in AlH_3 under pressure

Bruno Rousseau[1,2,*] and Aitor Bergara[1,2,3,†]

[1] *Donostia International Physics Center (DIPC), Paseo de Manuel Lardizabal, 20018, Donostia, Basque Country, Spain*
[2] *Centro de Fisica de Materiales CSIC-UPV/EHU, 1072 Posta kutxatila, E-20080 Donostia, Basque Country, Spain*
[3] *Materia Kondentsatuaren Fisika Saila, Zientzia eta Teknologia Fakultatea, Euskal Herriko Unibertsitatea, 644 Postakutxatila,48080 Bilbo, Basque Country, Spain*

(Dated: June 24, 2010)

The anharmonic self energy of two zone boundary phonons were computed to lowest order for AlH_3 in the $Pm\bar{3}n$ structure at 110 GPa. The wavevector and branch index corresponding to these modes are situated in a region of phase space providing most of the electron-phonon coupling. The self energies are found to be very large and the anharmonic contribution to the linewidth of one of the modes studied could be distinguished from the electron-phonon linewidth. It is found that anharmonicity suppresses the electron-phonon coupling parameter λ, providing a possible explanation for the disagreement between experiment and previous theoretical studies of superconductivity in this system.

I. INTRODUCTION

It has been suggested four decades ago that elemental hydrogen could form an exceptionally high T_c superconductor under compression[1] (a recent estimate being 242 K at 450 GPa[2]), and more recently that it could have very exotic properties, such as being a metallic quantum liquid[3], or forming protonic Cooper pairs[3,4]. However, metallic hydrogen has long been elusive; the dimers persist[5] and hydrogen remains non-metallic up to a pressure of 320 GPa[6].

An alternative route to hydrogen superconductivity has been suggested in the form of hydrides, where the presence of a heavier element can act to chemically "precompress" hydrogen, compelling it to reveal its superconducting properties at lower pressures[7,8]. Because of their large hydrogen content, superconductivity in the group IV hydrides has been studied extensively[9–15]. Some tri-hydrides also received attention recently[16] and it was suggested that the origin of superconductivity in these systems could be soft phonons in the vicinity of phase transitions. Within this context, aluminum hydride (AlH_3) under pressure has recently been studied both theoretically[17–19] and experimentally[19]. Using random structure searching, a particularly interesting phase of symmetry $Pm\bar{3}n$ has been found to be energetically favorable above $\sim$70 GPa[17,19]. This phase contains two formula units per cell, with the Al ions forming a body-centered-cubic (bcc) structure and the hydrogen ions forming linear chains on the faces of the cubic cell. *Ab initio* calculations also suggested that the electron-phonon coupling parameter should be fairly large in this phase at $\sim$110 GPa ($\lambda \simeq 0.74$), predicting a value of $T_c \simeq 24$ K,[19] in agreement with the general idea that compressed hydrides could be good superconductors[7]. Very interestingly, however, no superconducting transition was found down to 4 K[19]; the reason for the disagreement between theory and experiment is unclear.

In the present work, we show that the phonon modes which provide most of the electron-phonon coupling are actually strongly renormalized by anharmonicity, which should greatly affect the value of the predicted T_c.

In sections II and III, basic formulas pertaining to phonon mediated superconductivity and phonon anharmonicity are reminded, which also serves to fix the notation. The *ab initio* calculations performed are described in section IV, and the main results pertaining to anharmonicity are presented in section V.

II. SUPERCONDUCTIVITY

The theory of phonon-mediated superconductivity is well understood[20]. A popular approximation to the superconducting transition temperature is given by the Allen-Dynes modification of the McMillan formula,[21,22]

$$k_B T_c = \frac{\hbar\omega_{log}}{1.2} \exp\Big[-\frac{1.04(1+\lambda)}{\lambda-\mu^*(1+0.62\lambda)}\Big], \qquad (1)$$

where μ^* is a parameter of order 0.1 which approximately accounts for the electron-electron repulsion at the Fermi level (which tends to weaken Cooper pairs, and thus reduce T_c), ω_{log} is the logarithmic average of the phonon frequencies and λ is the electron-phonon interaction (or electronic mass enhancement) parameter. This last parameter in turn is obtained from the Eliashberg spectral function α^2F,

$$\lambda = \int_0^\infty d\omega \lambda(\omega); \qquad \lambda(\omega) = 2\frac{\alpha^2F(\omega)}{\omega}. \qquad (2)$$

The Eliashberg spectral function can be approximately related to the phonon linewidths $\gamma_\nu(\mathbf{q})$ by[23]

$$\alpha^2F(\omega) \simeq \frac{1}{2\pi\hbar}\frac{1}{N(\epsilon_F)}\frac{1}{N}\sum_{\mathbf{q},\nu}\frac{\gamma_\nu(\mathbf{q})}{\omega_\nu(\mathbf{q})}\delta\big(\omega-\omega_\nu(\mathbf{q})\big), \qquad (3)$$

where N is the number of unit cells in the crystal, $N(\epsilon_F)$ is the density of states per unit cell at the Fermi energy,

$\mathbf{q}$ is a wave vector constrained to the first Brillouin zone (1BZ), ν is a mode label and $\omega_\nu(\mathbf{q})$ is the frequency of phonon mode $\mathbf{q}\nu$. This implies that λ can also be expressed as

$$\lambda = \frac{1}{N}\sum_{\mathbf{q},\nu}\lambda_{\mathbf{q}\nu}, \tag{4}$$

with

$$\lambda_{\mathbf{q}\nu} = \frac{1}{\pi\hbar}\frac{1}{N(\epsilon_F)}\frac{\gamma_\nu(\mathbf{q})}{\omega_\nu(\mathbf{q})^2}. \tag{5}$$

The usual method employed to obtain λ from *ab initio* calculations is to first obtain the band structure of the system, second to obtain the phonon frequencies within the Born-Oppenheimer approximation, and third to obtain effective electron-phonon coupling parameters. The system is then approximately described in terms of a Fröhlich Hamiltonian,

$$\hat{H} = \sum_{n\mathbf{k}\sigma}\epsilon_{n\mathbf{k}}\hat{c}^\dagger_{n\mathbf{k}\sigma}\hat{c}_{n\mathbf{k}\sigma} + \sum_{\mathbf{q}\nu}\hbar\omega_\nu(\mathbf{q})\Big(\hat{b}^\dagger_{\mathbf{q}\nu}\hat{b}_{\mathbf{q}\nu}+\frac{1}{2}\Big) \tag{6}$$
$$+\frac{1}{\sqrt{N}}\sum_{\mathbf{q}\nu}\sum_{m,n\mathbf{k}\sigma}\hat{c}^\dagger_{m\mathbf{k}+\mathbf{q}\sigma}\hat{c}_{n\mathbf{k}\sigma}\Big(\hat{b}^\dagger_{-\mathbf{q}\nu}+\hat{b}_{\mathbf{q}\nu}\Big)g^{\nu\mathbf{q}}_{m\mathbf{k}+\mathbf{q},n\mathbf{k}},$$

the parameters of which are set to the *ab initio* computed values. In the above m,n are band labels, σ is a spin label, $\mathbf{k},\mathbf{q}$ are wave vectors in the 1BZ, $\{\hat{c},\hat{c}^\dagger\}$ and $\{\hat{b},\hat{b}^\dagger\}$ are electron and phonon ladder operators, $\{\epsilon\}$ are electronic eigenvalues and $\{g\}$ describe the strength of the scattering between electrons and phonons. It is standard to set the electronic energies to the Kohn-Sham eigenvalues, the phonon frequencies to the Born-Oppenheimer frequencies and to extract the values of the g parameters from the deformation potential. Standard field theory methods[24] are then employed to derive the phonon linewidths, γ_ν, from this Hamiltonian.

III. PHONON ANHARMONICITY

The position operator for the ions in a crystal can be represented as

$$\hat{\mathbf{r}}_\kappa(\mathbf{R}) = \mathbf{R} + \mathbf{b}_\kappa + \hat{\mathbf{u}}_\kappa(\mathbf{R}), \tag{7}$$

where $\mathbf{R}$ is a lattice vector, $\mathbf{b}_\kappa$ is the basis vector for ion κ and $\hat{\mathbf{u}}_\kappa(\mathbf{R})$ is the operator representing the displacement of the ion from its equilibrium position. Within the adiabatic approximation, which assumes the electronic system instantaneously adapts to the ionic positions, the total energy as a function of the ionic positions can be taken as an effective potential for the ions which thus dictates their dynamics. This potential is expressed as

$$\hat{U}[\{\hat{\mathbf{u}}\}] = U_0 + \sum_{n=2}^{\infty}\hat{U}_n[\{\hat{\mathbf{u}}\}], \tag{8}$$

with

$$\hat{U}_n[\{\hat{\mathbf{u}}\}] = \frac{1}{n!}\sum_{\{\alpha\kappa\mathbf{R}\}}\hat{u}^{\alpha_1}_{\kappa_1}(\mathbf{R}_1)...\hat{u}^{\alpha_n}_{\kappa_n}(\mathbf{R}_n)$$
$$\times\Phi^{\alpha_1...\alpha_n}_{\kappa_1...\kappa_n}(\mathbf{R}_1,...,\mathbf{R}_n), \tag{9}$$

where the Greek symbols $\alpha_1,...,\alpha_n$ represent cartesian coordinates. It is assumed that the crystal is stable and that, consequently, the linear term in the displacements vanishes identically. The dynamics of the ionic degrees of freedom are then described by the effective Hamiltonian

$$\hat{H} = \hat{T} + \hat{U}, \tag{10}$$

where $\hat{T}$ is the kinetic energy operator of the ions. It is convenient to consider a canonical change of variable to reciprocal space of the form

$$\hat{\mathbf{u}}_\kappa(\mathbf{R}) = \frac{1}{\sqrt{N}}\sum_{\mathbf{q}}e^{i\mathbf{q}\cdot\mathbf{R}}\hat{\mathbf{u}}_\kappa(\mathbf{q}) \tag{11}$$

In terms of these new position-like variables, the potential terms can be expressed as

$$\hat{U}_n[\{\hat{\mathbf{u}}\}] = \frac{1}{n!}\frac{1}{N^{\frac{n}{2}-1}}\sum_{\{\alpha\kappa\mathbf{q}\}}\hat{u}^{\alpha_1}_{\kappa_1}(\mathbf{q}_1)...\hat{u}^{\alpha_n}_{\kappa_n}(\mathbf{q}_n)$$
$$\times\Phi^{\alpha_1...\alpha_n}_{\kappa_1...\kappa_n}(-\mathbf{q}_1,...,-\mathbf{q}_n); \tag{12}$$

some useful symmetry relations pertaining to these anharmonic coefficients are reminded in appendix A.

A. Harmonic phonons

If the potential energy expansion is truncated after the second order, the resulting approximate Hamiltonian is harmonic, and leads to the standard small oscillations problem. In this case:

$$\hat{U}_2 = \frac{1}{2}\sum_{\{\alpha\kappa\}}\sum_{\mathbf{q}}\Big[\hat{u}^{\alpha_1}_{\kappa_1}(\mathbf{q})\Big]^\dagger D^{\alpha_1\alpha_2}_{\kappa_1\kappa_2}(\mathbf{q})\hat{u}^{\alpha_2}_{\kappa_2}(\mathbf{q}), \tag{13}$$

where the usual dynamical matrix has been defined as

$$D^{\alpha_1\alpha_2}_{\kappa_1\kappa_2}(\mathbf{q}) \equiv \Phi^{\alpha_1\alpha_2}_{\kappa_1\kappa_2}(\mathbf{q},-\mathbf{q}). \tag{14}$$

It is standard to consider a canonical transformation to ladder operators of the form

$$\hat{u}^\alpha_\kappa(\mathbf{q}) = \sum_\nu x^\alpha_{\kappa\nu}(\mathbf{q})\hat{A}_{\mathbf{q}\nu}; \qquad \hat{A}_{\mathbf{q}\nu} = \hat{b}_{\mathbf{q}\nu} + \hat{b}^\dagger_{-\mathbf{q}\nu}. \tag{15}$$

The displacement vectors are defined as

$$\mathbf{x}_{\kappa\nu}(\mathbf{q}) = \sqrt{\frac{\hbar}{2M_\kappa\omega_\nu(\mathbf{q})}}\mathbf{E}_{\kappa\nu}(\mathbf{q}), \tag{16}$$

where M_κ is the mass of ion κ and the polarization vectors $\mathbf{E}$, which are chosen to be orthonormal, are solutions of the hermitian eigenvalue problem

$$\sum_{\kappa_2\alpha_2}\frac{D^{\alpha_1\alpha_2}_{\kappa_1\kappa_2}(\mathbf{q})}{\sqrt{M_{\kappa_1}M_{\kappa_2}}}E^{\alpha_2}_{\kappa_2\nu}(\mathbf{q}) = \omega_\nu(\mathbf{q})^2E^{\alpha_1}_{\kappa_1\nu}(\mathbf{q}), \tag{17}$$

which also yields the harmonic phonon frequencies. It is useful to define a "mode mass" M_ν as

$$M_\nu(\mathbf{q}) = \frac{\sum_\kappa M_\kappa |\mathbf{x}_{\kappa\nu}(\mathbf{q})|^2}{\sum_\kappa |\mathbf{x}_{\kappa\nu}(\mathbf{q})|^2}; \tag{18}$$

this quantity is then a gauge of what type of ions are involved in a given mode. The harmonic part of the ionic Hamiltonian can finally be expressed as

$$\hat{H}_h = \hat{T} + \hat{U}_2, \tag{19}$$

$$= \sum_{\mathbf{q},\nu} \hbar\omega_\nu(\mathbf{q})\Big(\hat{b}^\dagger_{\mathbf{q}\nu}\hat{b}_{\mathbf{q}\nu} + \frac{1}{2}\Big). \tag{20}$$

B. Phonon-phonon interaction

When the anharmonic contributions to the potential cannot be neglected, the ionic Hamiltonian can be expressed in terms of the harmonic Hamiltonian plus phonon-phonon interaction terms. The anharmonic coefficients can be expressed in terms of the harmonic basis, and lowest order contributions to the self-energy anharmonic correction for the mode $(\mathbf{q}\nu)$ are given by[25]

$$\Pi^{(L)}_\nu(\mathbf{q},\omega) = \frac{1}{2N}\sum_{\nu_1,\mathbf{q}_1} \Phi_{\nu,\nu,\nu_1,\nu_1}(\mathbf{q},-\mathbf{q},\mathbf{q}_1,-\mathbf{q}_1)\left(2n_B\Big(\hbar\omega_{\nu_1}(\mathbf{q}_1)\Big)+1\right), \tag{21}$$

$$\Pi^{(T)}_\nu(\mathbf{q},\omega) = -\frac{1}{N}\sum_{\mathbf{q}_1}\sum_{\nu_1\nu_2} \Phi_{\nu_1,\nu_1,\nu_2}(-\mathbf{q}_1,\mathbf{q}_1,\mathbf{0})\Phi_{\nu_2,\nu,\nu}(\mathbf{0},\mathbf{q},-\mathbf{q})\frac{2n_B\Big(\hbar\omega_{\nu_1}(\mathbf{q}_1)\Big)+1}{\hbar\omega_{\nu_2}(\mathbf{0})}, \tag{22}$$

$$\Pi^{(B)}_\nu(\mathbf{q},\omega) = -\frac{1}{2N}\sum_{\mathbf{q}_1,\mathbf{q}_2}\sum_{\nu_1\nu_2}\sum_{\mathbf{G}} \delta_{\mathbf{q}_1+\mathbf{q}_2+\mathbf{q},\mathbf{G}}|\Phi_{\nu,\nu_1,\nu_2}(\mathbf{q},\mathbf{q}_1,\mathbf{q}_2)|^2 F\Big(\omega,\omega_{\nu_1}(\mathbf{q}_1),\omega_{\nu_2}(\mathbf{q}_2)\Big), \tag{23}$$

where

$$F(\omega,\omega_1,\omega_2) = \frac{1}{\hbar}\left[\frac{2\Big(\omega_1+\omega_2\Big)\Big(1+n_B(\omega_1)+n_B(\omega_2)\Big)}{\Big(\omega_1+\omega_2\Big)^2-\Big(\omega+i\delta\Big)^2} + \frac{2\Big(\omega_1-\omega_2\Big)\Big(n_B(\omega_2)-n_B(\omega_1)\Big)}{\Big(\omega_2-\omega_1\Big)^2-\Big(\omega+i\delta\Big)^2}\right] \tag{24}$$

and

$$\Phi_{\nu_1\ldots\nu_n}(\mathbf{q}_1,...,\mathbf{q}_n) = \sum_{\{\alpha\kappa\}} \Phi^{\alpha_1\ldots\alpha_n}_{\kappa_1\ldots\kappa_n}(\mathbf{q}_1,...,\mathbf{q}_n)x^{\alpha_1}_{\kappa_1\nu_1}(-\mathbf{q}_1)...x^{\alpha_n}_{\kappa_n\nu_n}(-\mathbf{q}_n). \tag{25}$$

In the above, the quantity n_B refers to the usual bosonic occupation factor. The labels $(T),(L)$ and (B) refer to the "tadpole", "loop" and "bubble" diagrams, as schematically represented in Figure 1. It is noteworthy that only the "bubble" contribution actually depends on the frequency ω, and that only this term will have an imaginary contribution. Furthermore, the "tadpole" diagram vanishes by symmetry in this system. The results above will be specialized to the point $\mathbf{q}_X = \pi/a(0,0,1)$ on the side of the zone, at zero temperature.

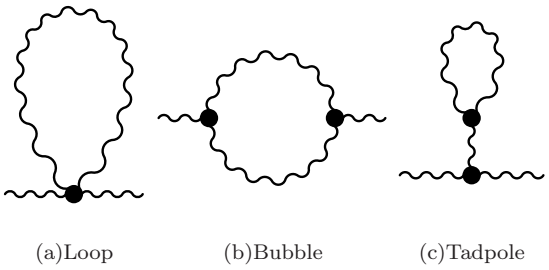

FIG. 1. Lowest order anharmonic self-energy diagrams. The lines represent phonon propagators and the vertices third order ("bubble" and "tadpole") and fourth order ("loop") anharmonic coupling.

IV. COMPUTATIONAL DETAILS

Electronic properties were computed using density functional theory (DFT) as implemented in the Quantum-ESPRESSO package[26]. The exchange-correlation was treated using the generalized gradient approximation (GGA) of Perdew, Burke and Ernzerhof (PBE)[27,28]. Ultrasoft pseudopotentials[29] were used, where $3s$ and $3p$ states of aluminium were treated as valence. The plane-wave basis cutoff was set to 80 Ry. First Brillouin Zone (1BZ) integrations were performed as sums on a $24\times24\times24$ Monkhorst-Pack $\mathbf{k}$-mesh, using a smearing parameter of 20 mRy. Phonon properties were computed using density-functional perturbation theory (DFPT)[26,30]. Interatomic force constants (IFC) were obtained from dynamical matrices computed on a

$12 \times 12 \times 12$ **q**-mesh. The electron-phonon coupling computations were performed using electronic and phonon quantities interpolated on a fine $72 \times 72 \times 72$ mesh.

V. RESULTS

The phonon dispersion was calculated for the $Pm\bar{3}n$ structure with a lattice constant $a = 5.82\,a_0$, which yielded a computed pressure of 109 GPa. The phonon spectral function α^2F, as well as the electron-phonon coupling parameter λ were also computed; results can be seen in Fig. 2. The values we have obtained are $\lambda \simeq 0.61$ and $\hbar\omega_{log} \simeq 68\,\text{meV}$, leading to $12\,\text{K} \lesssim T_c \lesssim 19\,\text{K}$ ($0.14 \geq \mu^* \geq 0.1$). As is clear from Fig. 2, the bulk of the contribution to λ comes from narrow regions in the 1BZ centered at X, for modes at $\sim 20\,\text{meV}$ and $\sim 85\,\text{meV}$; attention has been focused on the relevant modes at X, assuming that they are representative of modes in that region of the 1BZ. These doubly degenerate modes will henceforth be referred to as X_1 (20 meV) and X_2 (85 meV) and will be labelled as ν_X. Interestingly, for these modes the motion of hydrogen ions is perpendicular to their chains; the displacements for X_2 are mostly that of hydrogen ions (with a mode mass of 1.1 M_H), whereas the displacements of X_1 involve both types of ions (mode mass of 5.7 M_H).

To better understand the origin of the large contribution to λ of modes around X, frozen phonon-perturbed bands were computed for X_1 and X_2. A displacement of the form

$$\mathbf{u}_\kappa(\mathbf{R};\eta) = \eta e^{i\mathbf{q}_X\cdot\mathbf{R}}\mathbf{x}_{\kappa\nu_X}(\mathbf{q}_X) \tag{26}$$

was imposed on the ions in a supercell geometry for various values of the unitless parameter[31] η (the displacement can be chosen to be real because of the symmetry of the $\mathbf{q_X}$ point). The appropriate supercell corresponds to a doubling of the original cell along the c axis, yielding a tetragonal cell. In the presence of this frozen-in perturbation, the Kohn Sham Hamiltonian can be expressed to first order in η as

$$\hat{h}_{KS} \simeq \sum_{n\mathbf{k}\sigma}\Big[\epsilon_{n\mathbf{k}}\hat{c}^\dagger_{n\mathbf{k}\sigma}\hat{c}_{n\mathbf{k}\sigma} + \eta\sum_m \hat{c}^\dagger_{m\mathbf{k}+\mathbf{q}_X\sigma}\hat{c}_{n\mathbf{k}\sigma}g^{\nu_X\mathbf{q}_X}_{m\mathbf{k}+\mathbf{q}_X,n\mathbf{k}}\Big]. \tag{27}$$

The correction to the eigenenergies $\epsilon_{n\mathbf{k}}$ will be of order η^2 at a generic $\mathbf{k}$ point. However, in the case of band degeneracy, the usual response formalism breaks down and the change in the band energy can be linear in η. The unperturbed cubic system has Fermi sheets centered at the R (doubly degenerate) and M (non degenerate) points. As can be seen in Fig. 3, these two Fermi sheets are centered about the M point in the supercell geometry. The two sets of bands intersect close to the Fermi energy along the Γ-M direction at a point $\mathbf{k}_0$; at this point, the Kohn Sham Hamiltonian can be modeled, to linear order in η, as

$$\mathbf{h}_{KS} = \begin{pmatrix} \epsilon_0 & 0 & \eta g \\ 0 & \epsilon_0 & \eta g \\ \eta g^* & \eta g^* & \epsilon_0 \end{pmatrix}, \tag{28}$$

where

$$\epsilon_0 \equiv \epsilon_{n\mathbf{k}_0}; \qquad g \equiv g^{\nu_X\mathbf{q_X}}_{m\mathbf{k}_0+\mathbf{q_X},n\mathbf{k}_0}. \tag{29}$$

The band label indicates one of the three $\eta = 0$ degenerate states, and it is assumed that the only relevant coupling to linear order is between the non-degenerate M band and the doubly degenerate R bands. The eigenvalues of this Hamiltonian matrix are given by

$$\epsilon = 0, \pm\sqrt{2}\eta|g| \tag{30}$$

and it is straightforward to extract a value for $|g|$. We find that $|g| \simeq 440\,\text{meV}$ for X_1 and $|g| \simeq 470\,\text{meV}$ for X_2. These couplings are very large on the phonon energy scale, and suggest that the origin of the large linewidths lies in strong scattering between the Fermi sheets mentioned above. The large coupling associated to X_1 and X_2 prompted further investigation of these modes.

In order to gauge the anharmonicity of these modes, total energy frozen phonon calculations were also performed. A displacement of the form given by Eq. (26) corresponds to

$$u^\alpha_\kappa(\mathbf{q};\eta) = \eta\sqrt{N}x^\alpha_{\kappa\nu_X}(\mathbf{q}_X)\delta_{\mathbf{q},\mathbf{q_X}}. \tag{31}$$

It is important to note that, for a finite value of η, this does not correspond to a realistic configuration of the ions. Indeed, the zero-point energy of a mode is in the order of meV, an energy that must be shared by all ions (a number of order N). Thus, for a single mode, only an infinitesimal amount of energy can be assigned to any ion, leading to infinitesimal average displacement. It is then the sum on all modes that yield a finite average displacement for any ion. This discussion does not invalidate the frozen phonon calculations, as they are only performed to extract anharmonic coefficients.

According to the expressions for the anharmonic energy as a function of displacement, Eq. (8) and (12), the total energy per unit cell for a given displacement should then be

$$\frac{U[\eta]}{N} = \frac{U_0}{N} + \frac{\eta^2}{4}\hbar\omega_{\nu_X}(\mathbf{q}_X) + \frac{\eta^4}{24}\Phi_{4,\nu_X} + O(\eta^6) \tag{32}$$

where

$$\Phi_{4,\nu_X} = \Phi_{\nu_X\nu_X\nu_X\nu_X}(\mathbf{q}_X,\mathbf{q}_X,\mathbf{q}_X,\mathbf{q}_X) \tag{33}$$

has been defined for convenience (note that $\mathbf{q}_X$ and $-\mathbf{q}_X$ are equivalent points by reciprocal lattice periodicity). It is straightforward to extract the values of $\hbar\omega_{\nu_X}(\mathbf{q}_X)$ and Φ_{4,ν_X} from the energy as a function of η using a finite difference scheme; results can be seen in figure 4. As can be seen on the figure, the quartic contribution to the

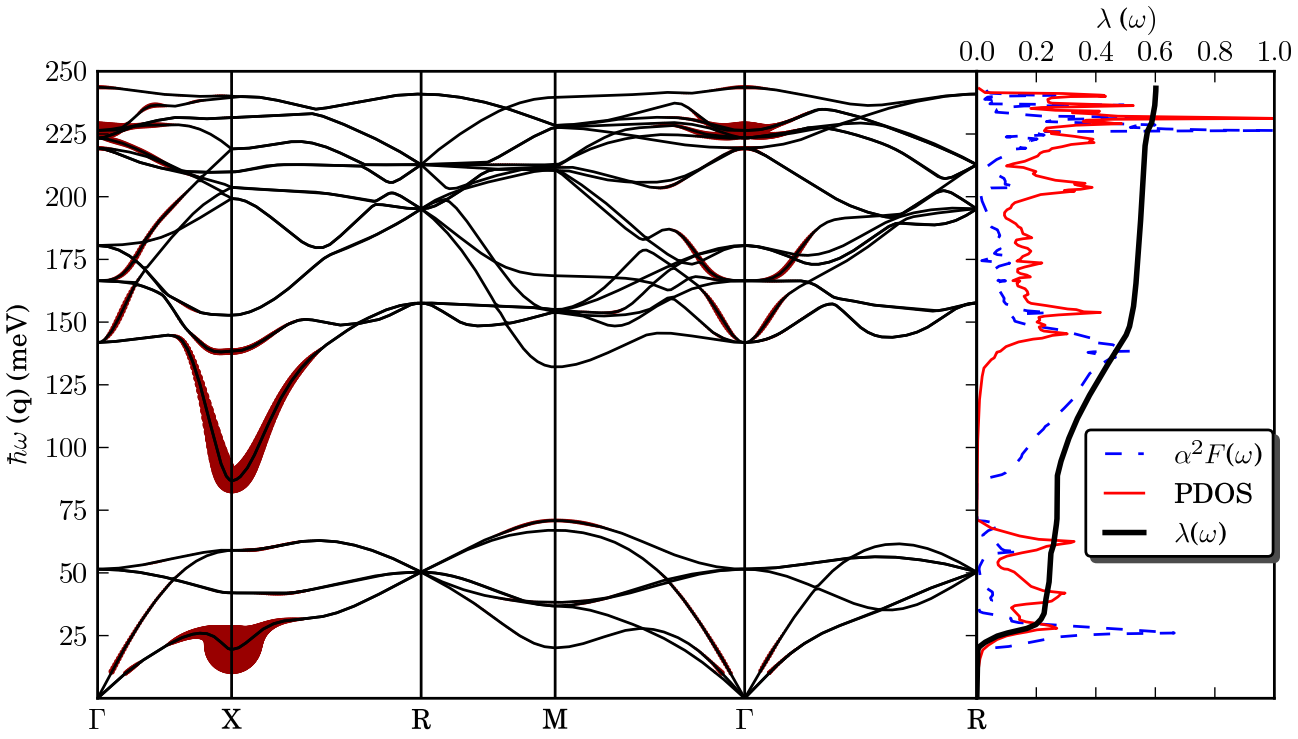

FIG. 2. (Color online) (Left panel) Phonon dispersion relation computed using DFPT. The areas of the red circles overlapping the phonon dispersion are proportional to $\lambda_{\nu\mathbf{q}}$. It is clear that the bulk of the electron phonon coupling can be attributed to modes in a region near X with frequencies $\sim 20\,\mathrm{meV}(\mathrm{X}_1)$ and $\sim 85\,\mathrm{meV}(\mathrm{X}_2)$. (Right panel) Eliashberg spectral function and phonon density of states PDOS (both in arbitrary units), as well as partially integrated value of λ.

potential is very large, with $\Phi_4 \simeq 155\,\mathrm{meV}$ for X_1 and $\Phi_4 \simeq 223\,\mathrm{meV}$ for X_2. In the *naive* approximation that the quartic anharmonic coupling is constant throughout the zone and that coupling to other modes can be neglected, namely

$$\Phi_{\nu_X,\nu_X,\nu,\nu}(\mathbf{q}_X,\mathbf{q}_X,\mathbf{q},-\mathbf{q}) \simeq \delta_{\nu,\nu_X}\Phi_{\nu_X,\nu_X,\nu_X,\nu_X}(\mathbf{q}_X,\mathbf{q}_X,\mathbf{q}_X,\mathbf{q}_X), \quad (34)$$

and at zero temperature, this leads to a frequency renormalization through the "loop" diagram of 77 meV for X_1 and 111 meV for X_2 (see equation 21).

Drawing conclusions from results at a single $\mathbf{q}$ point can be premature, as is examplified by the case of MgB_2: frozen phonon calculations similar to those presented above suggested that the E_{2g} modes at Γ should be highly anharmonic[32]; refined calculations of the "loop" and "bubble" diagrams for this mode revealed that in fact this is not the case[33,34]. The point is that a frozen phonon calculation provides no information on the cubic coupling, which can largely cancel the quartic contribution, nor does it account for the fact that the anharmonic coefficients have dispersions (*ie* are functions of $\mathbf{q}$). Nevertheless, the unusually large value of Φ_4 prompted a more thorough investigation of anharmonicity for these modes.

	$\hbar\omega_\nu(\mathbf{q}_X)$		Φ_{4,ν_X}	
	FP	DFPT	FP	SFD
X_1	19.5	19.4	154.6	154.9
X_2	86.9	86.8	222.8	224.2

TABLE I. Comparing harmonic frequencies and Φ_4 parameters (in meV) obtained by different methods. DFPT means "density functional perturbation theory", FP means "frozen phonon" and SFD means "supercell finite difference". Results are seen to agree very well between different calculations, giving confidence on the convergence of the SFD method.

The necessary coefficients were obtained by finite differencing of dynamical matrices computed for appropriate supercells (henceforth the "supercell finite difference", of SFD, method); a complete discussion of the formalism can be found in appendix B. Briefly, anharmonic parameters were obtained by computing dynamical matrices with ions slightly displaced according to the polarizations of modes X_1 and X_2. A centered, five points finite difference scheme was applied to these dynamical matrices, yielding partially mode-projected anharmonic

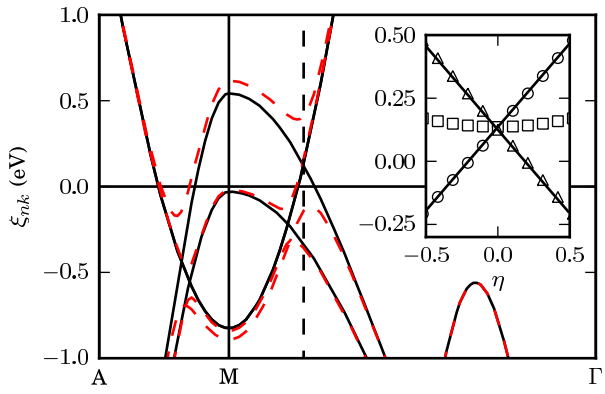

FIG. 3. (Color online) Electronic bands near the Fermi energy in the tetragonal supercell. The bands for the unperturbed structure are shown (full black line), as well as for a X_2 frozen phonon displacement corresponding to $\eta \simeq 0.4$ (dashed red line). The zero of energy is set at the Fermi energy of the unperturbed system. The X_1 data is not significantly different. The dashed vertical line indicates the point $\mathbf{k}_0$ where the unperturbed bands cross. (Inset) Perturbed eigenvalues as a function of η corresponding to the degenerate energy indicated by the dashed line. The splitting is linear with the distortion for two bands (circles and triangles) and remains quadratic for the third (squares); the value of $|g|$: is directly related to the slope of the change in band energy with η, and is equal to ~ 470 meV in this case.

	$\Pi_\nu^{(L)}$	$\Pi_\nu^{(B)}$	Π_ν	$\hbar\omega_\nu$	$\hbar\Omega_\nu$	shift (%)
X_1	22.9	−6.3	16.6	19.4	31.9	65
X_2	37.3	−12.0	24.9	86.8	108.9	25

TABLE II. Computed values of the self-energy corrections for modes X_1 and X_2, at zero temperature and zero frequency, and comparison of the renormalized frequency, Ω_ν, with the harmonic frequency ω_ν. All energies are in meV. The relative shift is seen to be quite large.

coefficients of the form $\Phi^{\alpha_1\alpha_2}_{\kappa_1\kappa_2;\nu_X}(\mathbf{q})$ and $\Phi^{\alpha_1\alpha_2}_{\kappa_1\kappa_2;\nu_X\nu_X}(\mathbf{q})$. These coefficients were obtained on a $4\times4\times4$ $\mathbf{q}$-mesh; Fourier interpolation was used to approximate them throughout the 1BZ.

The frequency dependent self-energy was computed in a range of interest, and the phonon spectral function was obtained[24]. In particular, by using the Lehmann representation[24], it can be shown that

$$\int_0^\infty d\omega \frac{B_\nu(\mathbf{q},\omega)}{\omega} = \frac{\omega_\nu(\mathbf{q})}{\Omega_\nu(\mathbf{q},0)^2}, \tag{35}$$

where

$$\Big(\hbar\Omega_\nu(\mathbf{q},\omega)\Big)^2 = \Big(\hbar\omega_\nu(\mathbf{q})\Big)^2 + 2\hbar\omega_\nu\Pi_\nu(\mathbf{q},\omega). \tag{36}$$

The computed values of the "loop" and "bubble" self energy diagrams, at zero temperature and zero frequency, can be seen in Table II, along with the values of $\Omega_\nu(\mathbf{q}_X,0)$. The "loop" contributions are quite large, but 3 to 4 times smaller than what the *naive* estimate based on dipsersionless parameters suggested. The cubic terms, which are real and negative at zero frequency, further reduce the estimate of the total self energy. The latter remains large enough however to strongly renormalize Ω_ν with respect to ω_ν, yielding a sizeable relative shift of 65 % (25 %) of the frequency of mode X_1 (X_2).

The contributions to the linewidths coming from anharmonic effects were also computed at 0 and 300 K, for a *fixed* lattice geometry (a fixed value of a). Although a proper analysis of the temperature dependence should include the lattice expansion (which is beyond the scope of this work), we expect that the fixed cell calculations should still be indicative of the behavior of the linewidths at fixed pressure. The widths were found to be vanishingly small (0.3 meV) for mode X_1 and 0.6 meV (4.6 meV) for mode X_2 at 0 K (300 K). Given that the electron-phonon contribution to the linewidth at X_2 is about 10 meV, it should be possible to observe the temperature dependent contribution to this mode's linewidth, providing a possible experimental signature of the effects described here.

In the approximation that anharmonicity does not affect the electron-phonon coupling (a reasonable assumption given that the g parameters are obtained from the deformation potential method, which is not affected by anharmonicity), the mode coupling is renormalized by anharmonicity and becomes

$$\lambda^{(anh)}_{\mathbf{q}\nu} = \frac{1}{\pi\hbar N(0)}\frac{\gamma_\nu(\mathbf{q})}{\Omega_\nu(\mathbf{q},0)^2}. \tag{37}$$

A complete calculation of the renormalized value $\lambda^{(anh)}$ from equation (4) would require knowledge of the anharmonic coefficients at points other than $\mathbf{q_X}$ and is beyond the scope of this work. However we can estimate an upper bound for the effect of the anharmonicity on the electron-phonon coupling. From Fig. 2 it is reasonable to assume that the electron-phonon coupling from 0 to ~ 35 meV can be attributed to the region near X_1 (partial value $\lambda_1 \simeq 0.23$) and that the electron-phonon coupling from ~ 85 meV to ~ 135 meV can be attributed to the region near X_2 (partial value $\lambda_2 \simeq 0.2$); the rest of the coupling is lumped together and assumed unaffected by anharmonicity (partial value $\lambda_3 = \lambda - \lambda_1 - \lambda_2 \simeq 0.18$). By estimating that the harmonic Eliashberg function is composed of two properly normalized δ peaks at ω_1 and ω_2 (the frequencies corresponding to X_1 and X_2) plus features unaffected by anharmonicity away from these frequencies, the renormalized coupling is given by

$$\lambda^{(anh)} \simeq \left(\frac{\omega_1}{\Omega_1}\right)^2\lambda_1 + \left(\frac{\omega_2}{\Omega_2}\right)^2\lambda_2 + \lambda_3 = 0.39, \tag{38}$$

where Ω_1 and Ω_2 are the renormalized frequencies of X_1 and X_2. A similar treatment yield $\hbar\omega^{(anh)}_{log} \simeq 125$ meV; using these renormalized parameters, the Allen-Dynes modification to the McMillan formula yields $1.5\,\mathrm{K} \lesssim \mathrm{T}_c \lesssim 5\,\mathrm{K}$ for $0.14 \geq \mu^* \geq 0.1$, suggesting that the anharmonic renormalization of the phonon spectrum, which acts to

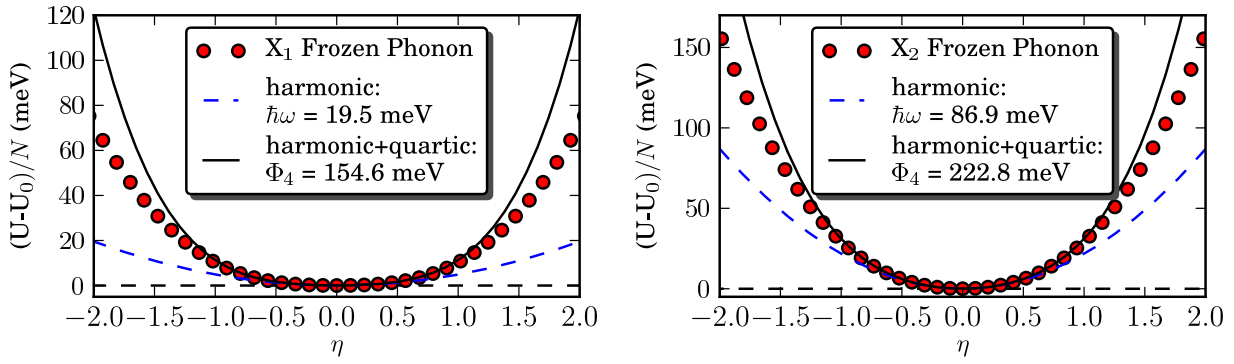

(a) X_1 (b) X_2

FIG. 4. (Color online) Frozen phonon total energy calculations for the modes at X with frequency ~ 20 meV (X_1) and ~ 85 meV (X_2), as a function of a displacement parameter η. The values of the parameters $\hbar\omega$ and Φ_4 are obtained from finite difference schemes.

stiffen the modes which provides most of the contribution to λ, leads to a strong reduction on T_c compared to the results obtained from the harmonic phonon spectrum.

VI. CONCLUSION

In this work, a full analysis of anharmonic effects to lowest order has been presented for modes in a region of the 1BZ which provides most of the contribution to λ, and this analysis has been compared to *naive* frozen phonon calculations. It has been shown that the modes X_1 and X_2 of AlH_3 are strongly renormalized by anharmonicity, although less so than a frozen phonon calculation might have suggested. Indeed, it is found that the frequency of X_1 is renormalized to 31.9 meV from 19.4 meV (a 65% shift) and that the frequency of X_2 is renormalized to 108.9 meV from 86.8 meV (a 25% shift). Furthermore, it is expected that anharmonicity induces a large, temperature dependent contribution to the X_2 mode linewidth, which could provide an experimental signature of the effect. A rough estimate suggests that renormalization could lead to a great reduction of the computed value of T_c, which could be as low as 2 K, compared to the harmonic prediction of $T_c \simeq 20$ K.

Thus, anharmonicity in AlH_3 might play a role in explaining why the measured and computed superconducting transition temperatures are in qualitative disagreement. There could be further phonon frequency renormalization due to the large electron-phonon coupling and, given that the electronic bandwidth near the Fermi energy is quite small, non-adiabatic effects in this system could also be substantial.

ACKNOWLEDGMENTS

We are grateful to I. Errea, J.M. Perez-Mato, and N.W. Ashcroft for fruitful discussions. We acknowledge financial support from UPV/EHU (Grant No. IT-366-07).

Appendix A: Symmetries of anharmonic coefficients

The anharmonic coefficients can be defined as

$$\Phi^{\alpha_1\ldots\alpha_n}_{\kappa_1\ldots\kappa_n}(\mathbf{R}_1,...,\mathbf{R}_n) = \left.\frac{\partial^n U[\{\mathbf{u}\}]}{\partial u^{\alpha_1}_{\kappa_1}(\mathbf{R}_1)...\partial u^{\alpha_n}_{\kappa_n}(\mathbf{R}_n)}\right|_{\mathbf{u}=\mathbf{0}} \quad \text{(A1)}$$

which immediately implies that they are real and symmetric under permutations of indices. Define the Fourier transformed coefficients as

$$\Phi^{\alpha_1\ldots\alpha_n}_{\kappa_1\ldots\kappa_n}(\mathbf{q}_1,...,\mathbf{q}_n) = \frac{1}{N}\sum_{\{\mathbf{R}\}} e^{-i(\mathbf{q}_1\cdot\mathbf{R}_1+\ldots+\mathbf{q}_n\cdot\mathbf{R}_n)} \times\Phi^{\alpha_1\ldots\alpha_n}_{\kappa_1\ldots\kappa_n}(\mathbf{R}_1,...,\mathbf{R}_n). \quad \text{(A2)}$$

Translational symmetry, which can be expressed as

$$\Phi^{\alpha_1\ldots\alpha_n}_{\kappa_1\ldots\kappa_n}(\mathbf{R}_1,...,\mathbf{R}_n) = \Phi^{\alpha_1\ldots\alpha_n}_{\kappa_1\ldots\kappa_n}(\mathbf{R}_1+\mathbf{R},...,\mathbf{R}_n+\mathbf{R}) \quad \text{(A3)}$$

for all lattice vectors $\mathbf{R}$, implies that $\Phi^{\alpha_1\ldots\alpha_n}_{\kappa_1\ldots\kappa_n}(\mathbf{q}_1,...,\mathbf{q}_n)$ vanishes unless $\mathbf{q}_1+...+\mathbf{q}_n$ is a reciprocal lattice vector. Furthermore,

$$\Phi^{\alpha_1\ldots\alpha_n}_{\kappa_1\ldots\kappa_n}(\mathbf{q}_1,...,\mathbf{q}_n) = \Phi^{\alpha_1\ldots\alpha_n}_{\kappa_1\ldots\kappa_n}(\mathbf{q}_1+\mathbf{G}_1,...,\mathbf{q}_n+\mathbf{G}_n) \quad \text{(A4)}$$

for any set of reciprocal lattice vectors $\{\mathbf{G}\}$.

Appendix B: Extracting anharmonic parameters from dynamical matrices

The lowest order anharmonic correction to the self energy,

$$\Pi = \Pi^{(L)} + \Pi^{(B)} + \Pi^{(T)}, \quad \text{(B1)}$$

involves anharmonic coefficients of third ("bubble" and "tadpole") and fourth ("loop") order. The most efficient and elegant way of obtaining these parameters is the use of the $2n+1$ theorem within the context of density-functional perturbation theory[30]. Briefly, this theorem guarantees that derivatives of the total energy up to order $2n+1$ can be obtained from knowledge of the derivatives of the wave-functions to order n. In practice, however, only the first order derivatives of the wavefunctions (*ie* $n=1$) are readily available, and finite-difference schemes are employed to obtain fourth order coefficients.

An alternative way of obtaining the necessary coefficients is through the frozen phonon method and finite differencing. What this method lacks in elegance, it makes up for by its simplicity and straightforward use, without the need for specialized software. The frozen phonon approach for this purpose is impractical for arbitrary $\mathbf{q}$ in the 1BZ, as it implies computations with potentially very large supercells. However, the interesting point in this case is $\mathbf{q}_X = \pi/a(0,0,1)$, which lies on the side of the zone.

Consider displacements of the ions from their equilibrium positions of the form

$$\Delta b_\kappa^\alpha(\mathbf{R};\eta) = \eta e^{i\mathbf{q}_X\cdot\mathbf{R}_i} x_{\kappa\nu}^\alpha(\mathbf{q}_X), \tag{B2}$$

where η is a small real number and ν is a specific mode of interest (X_1 or X_2). In Fourier space, this corresponds to

$$\Delta b_\kappa^\alpha(\mathbf{q};\eta) = \eta\delta_{\mathbf{q},\mathbf{q}_X}\sqrt{N}x_{\kappa\nu}^\alpha(\mathbf{q}_X). \tag{B3}$$

The positions of the ions, now considered as simple numbers and not operators, can be defined as

$$\mathbf{r}_\kappa(\mathbf{R}) = \mathbf{R} + \mathbf{b}_\kappa + \Delta\mathbf{b}_\kappa(\mathbf{R};\eta) + \mathbf{u}_\kappa(\mathbf{R}). \tag{B4}$$

The dynamical matrix computed about the non-equilibrium position is given by

$$D_{\kappa_1\kappa_2}^{\alpha_1\alpha_2}(\mathbf{q};\eta) = \frac{\partial^2}{\partial u_{\kappa_1}^{\alpha_1}(-\mathbf{q})\partial u_{\kappa_2}^{\alpha_2}(\mathbf{q})} U[\{\mathbf{u}+\Delta\mathbf{b}\}]\Big|_{\mathbf{u}=\mathbf{0}} \tag{B5}$$

$$= D_{\kappa_1\kappa_2}^{\alpha_1\alpha_2}(\mathbf{q}) + \frac{\eta^2}{2}\sum_{\kappa_3,\kappa_4}\sum_{\alpha_3,\alpha_4} x_{\kappa_3\nu}^{\alpha_3}(\mathbf{q}_X)x_{\kappa_4\nu}^{\alpha_4}(\mathbf{q}_X) \times\Phi_{\kappa_1\kappa_2\kappa_3\kappa_4}^{\alpha_1\alpha_2\alpha_3\alpha_4}(\mathbf{q},-\mathbf{q},\mathbf{q}_X,\mathbf{q}_X) + O(\eta^3); \tag{B6}$$

from this last expression it is clear that the coefficients of interest for the computation of the "loop" diagram can be extracted from the second derivative with respect to η of the out-of-equilibrium dynamical matrix.

The situation is slightly more complicated, however. The ionic displacements introduced do not have the periodicity of the lattice; such periodicity is essential in order to apply standard computational methods to extract the dynamical matrix. The displacements are periodic with respect to a lattice whose cells (henceforth supercell) contain two of the original cells stacked in the c direction. These subcells of the supercells will be labeled with $\delta=0$ and $\delta=1$. Define

$$\mathbf{A} = a(0,0,1); \tag{B7}$$

any lattice vector of the original lattice $\mathbf{R}$ can be expressed as

$$\mathbf{R} = \bar{\mathbf{R}} + \delta\mathbf{A} \tag{B8}$$

where $\bar{\mathbf{R}}$ is some vector of the superlattice and δ can be either 0 or 1. The ionic positions with respect to this new basis are expressed as

$$\bar{\mathbf{r}}_{(\kappa,\delta)}(\bar{\mathbf{R}}) = \bar{\mathbf{R}} + \delta\mathbf{A} + \mathbf{b}_\kappa + \eta e^{i\pi\delta}\mathbf{x}_\kappa + \bar{\mathbf{u}}_{(\kappa,\delta)}(\bar{\mathbf{R}}), \tag{B9}$$

where now the compound index (κ,δ) identifies all the ions in the supercell with a label indicating ion κ and subcell δ. In reciprocal space,

$$\bar{\mathbf{u}}_{(\kappa,\delta)}(\bar{\mathbf{R}}) = \sqrt{\frac{2}{N}}\sum_{\bar{\mathbf{q}}} e^{i\bar{\mathbf{q}}\cdot\bar{\mathbf{R}}}\bar{\mathbf{u}}_{(\kappa,\delta)}(\bar{\mathbf{q}}) \tag{B10}$$

where $\bar{\mathbf{q}}$ is a wave vector in the 1BZ of the superlattice. The following relationships are thus immediate:

$$\bar{\mathbf{u}}_{(\kappa,\delta)}(\bar{\mathbf{R}}) = \mathbf{u}_\kappa(\mathbf{R}=\bar{\mathbf{R}}+\delta\mathbf{A}) \tag{B11}$$

$$\bar{\mathbf{u}}_{(\kappa,\delta)}(\bar{\mathbf{q}}) = \frac{e^{i\delta\bar{\mathbf{q}}\cdot\mathbf{A}}}{\sqrt{2}}\Big(\mathbf{u}_\kappa(\bar{\mathbf{q}}) + e^{i\delta\pi}\mathbf{u}_\kappa(\bar{\mathbf{q}}+\mathbf{q}_X)\Big), \tag{B12}$$

which implies

$$\frac{\partial}{\partial\bar{u}_{(\kappa,\delta)}^\alpha(\bar{\mathbf{q}})} = \frac{e^{-i\delta\bar{\mathbf{q}}\cdot\mathbf{A}}}{\sqrt{2}}\Big(\frac{\partial}{\partial u_\kappa^\alpha(\bar{\mathbf{q}})} + e^{i\delta\pi}\frac{\partial}{\partial u_\kappa^\alpha(\bar{\mathbf{q}}+\mathbf{q}_X)}\Big). \tag{B13}$$

Above "$\bar{\mathbf{q}}+\mathbf{q}_X$" is meant to represent the wave vector inside the 1BZ of the original lattice which is obtained from $\bar{\mathbf{q}}+\mathbf{q}_X$ by an appropriate reciprocal lattice translation. For what follows, it will be useful to remember that $2\mathbf{q_X}$ is a reciprocal lattice vector of the original system, such that all anharmonic coefficients are periodic under $\mathbf{q}\to\mathbf{q}+2\mathbf{q_X}$.

The dynamical matrix in the supercell representation is given by

$$\bar{D}^{\alpha_1\alpha_2}_{(\kappa,\delta)_1,(\kappa,\delta)_2}(\bar{\mathbf{q}}) = \left.\frac{\partial^2 U[\{\bar{\mathbf{u}}\}]}{\partial \bar{u}^{\alpha_1}_{(\kappa,\delta)_1}(-\bar{\mathbf{q}})\partial \bar{u}^{\alpha_2}_{(\kappa,\delta)_2}(\bar{\mathbf{q}})}\right|_{\bar{\mathbf{u}}=\mathbf{0}} \tag{B14}$$

$$= \frac{e^{i(\delta_1-\delta_2)\bar{\mathbf{q}}\cdot\mathbf{A}}}{2}\left[D^{\alpha_1\alpha_2}_{\kappa_1\kappa_2}(\bar{\mathbf{q}};\eta) + e^{i(\delta_1+\delta_2)\pi}D^{\alpha_1\alpha_2}_{\kappa_1\kappa_2}(\bar{\mathbf{q}}+\mathbf{q}_X;\eta) + e^{i\delta_2\pi}O^{\alpha_1\alpha_2}_{\kappa_1\kappa_2}(\bar{\mathbf{q}};\eta) + e^{i\delta_1\pi}O^{\alpha_1\alpha_2}_{\kappa_1\kappa_2}(\bar{\mathbf{q}}+\mathbf{q}_X;\eta)\right], \tag{B15}$$

where

$$O^{\alpha_1\alpha_2}_{\kappa_1\kappa_2}(\bar{\mathbf{q}};\eta) = \left.\frac{\partial^2 U[\{\mathbf{u}\}]}{\partial u^{\alpha_1}_{\kappa_1}(-\bar{\mathbf{q}})\partial u^{\alpha_2}_{\kappa_2}(\bar{\mathbf{q}}+\mathbf{q}_X)}\right|_{\mathbf{u}=\mathbf{0}} = \eta\sum_{\kappa_3,\alpha_3}\Phi^{\alpha_1\alpha_2\alpha_3}_{\kappa_1\kappa_2\kappa_3}(\bar{\mathbf{q}},-\bar{\mathbf{q}}-\mathbf{q}_X,\mathbf{q}_X)x^{\alpha_3}_{\kappa_3\nu}(\mathbf{q}_X)+O(\eta^2), \tag{B16}$$

and

$$O^{\alpha_1\alpha_2}_{\kappa_1\kappa_2}(\bar{\mathbf{q}}+\mathbf{q}_X;\eta) = \left.\frac{\partial^2 U[\{\mathbf{u}\}]}{\partial u^{\alpha_1}_{\kappa_1}(-\bar{\mathbf{q}}-\mathbf{q}_X)\partial u^{\alpha_2}_{\kappa_2}(\bar{\mathbf{q}})}\right|_{\mathbf{u}=\mathbf{0}} = \eta\sum_{\kappa_3,\alpha_3}\Phi^{\alpha_1\alpha_2\alpha_3}_{\kappa_1\kappa_2\kappa_3}(\bar{\mathbf{q}}+\mathbf{q}_X,-\bar{\mathbf{q}},\mathbf{q}_X)x^{\alpha_3}_{\kappa_3\nu}(\mathbf{q}_X)+O(\eta^2). \tag{B17}$$

From these last two terms, the anharmonic coefficients necessary for the computation of the "bubble" diagram can be extracted.

Thus, from the supercell dynamical matrices $\bar{D}(\eta)$ (the quantities actually computed through DFPT), it is a simple matter of algebra to extract $D(\eta)$ and $O(\eta)$. It is then useful to define partially projected anharmonic parameters,

$$\Phi^{\alpha_1\alpha_2}_{\kappa_1\kappa_2;\nu_X\nu_X}(\mathbf{q}) \equiv \frac{\eta^2}{2}\sum_{\kappa_3,\kappa_4}\sum_{\alpha_3,\alpha_4}x^{\alpha_3}_{\kappa_3\nu}(\mathbf{q}_X)x^{\alpha_4}_{\kappa_4\nu}(\mathbf{q}_X) \times\Phi^{\alpha_1\alpha_2\alpha_3\alpha_4}_{\kappa_1\kappa_2\kappa_3\kappa_4}(\mathbf{q},-\mathbf{q},\mathbf{q}_X,\mathbf{q}_X) \tag{B18}$$

$$= \frac{\partial^2}{\partial\eta^2}D^{\alpha_1\alpha_2}_{\kappa_1\kappa_2}(\mathbf{q};\eta)+O(\eta), \tag{B19}$$

and

$$\Phi^{\alpha_1\alpha_2}_{\kappa_1\kappa_2;\nu_X}(\mathbf{q}) \equiv \eta\sum_{\kappa_3}\sum_{\alpha_3}x^{\alpha_3}_{\kappa_3\nu}(\mathbf{q}_X) \times\Phi^{\alpha_1\alpha_2\alpha_3}_{\kappa_1\kappa_2\kappa_3}(\mathbf{q},-\mathbf{q}-\mathbf{q_X},\mathbf{q}_X) \tag{B20}$$

$$= \frac{\partial}{\partial\eta}O^{\alpha_1\alpha_2}_{\kappa_1\kappa_2}(\mathbf{q};\eta)+O(\eta). \tag{B21}$$

These parameters can then straightforwardly be obtained by estimating the η derivatives by finite difference schemes. Furthermore, since these coefficients are periodic in reciprocal space (namely periodic under $\mathbf{q}\rightarrow\mathbf{q}+\mathbf{G}$), they are susceptible to Fourier interpolation, in complete analogy with the usual procedures employed with dynamical matrices. Once these coefficients are obtained on a dense $\mathbf{q}$ mesh, it is possible to compute the "loop" and "bubble" diagrams.

* sckrousb@ehu.es
† a.bergara@ehu.es

[1] N. W. Ashcroft, Phys. Rev. Lett., **21**, 1748 (1968).
[2] P. Cudazzo, G. Profeta, A. Sanna, A. Floris, *et al.*, Phys. Rev. Lett., **100**, 257001 (2008).
[3] E. Babaev, A. Sudbo, and N. W. Ashcroft, Phys. Rev. Lett., **95**, 105301 (2005).
[4] E. Babaev and N. W. Ashcroft, Nat. Phys., **3**, 530 (2007).
[5] K. Nagao, S. A. Bonev, A. Bergara, and N. W. Ashcroft, Phys. Rev. Lett., **90**, 035501 (2003).
[6] P. Loubeyre, F. Occelli, and R. LeToullec, Nature, **416**, 613 (2002).
[7] N. W. Ashcroft, Phys. Rev. Lett., **92**, 187002 (2004).
[8] J. Feng, W. Grochala, T. Jaroń, R. Hoffmann, *et al.*, Phys. Rev. Lett., **96**, 017006 (2006).
[9] G. Gao, A. R. Oganov, P. Li, Z. Li, *et al.*, PNAS, **26**, 1317 (2010).
[10] M. Martinez-Canales, A. R. Oganov, Y. Ma, Y. Yan, *et al.*, Phys. Rev. Lett., **102**, 087005 (2009).
[11] G. Gao, A. R. Oganov, A. Bergara, M. Martinez-Canales, *et al.*, Phys. Rev. Lett., **101**, 107002 (2008).
[12] M. Martinez-Canales, A. Bergara, J. Feng, and W. Grochala, J. Phys. Chem. Solids, **67**, 2095 (2006).
[13] O. Degtyareva, M. M. Canales, A. Bergara, X.-J. Chen, *et al.*, Phys. Rev. B, **76**, 064123 (2007).
[14] M. I. Eremets, I. A. Trojan, S. A. Medvedev, J. S. Tse, *et al.*, Science, **319**, 1506 (2008).
[15] X.-J. Chen, V. V. Struzhkin, Y. Song, A. F. Goncharov,

et al., PNAS, **105**, 20 (2008).
[16] D. Y. Kim, R. H. Scheicher, H. kwang Mao, T. W. Kang, *et al.*, PNAS, **107**, 2793 (2010).
[17] C. J. Pickard and R. J. Needs, Phys. Rev. B, **76**, 144114 (2007).
[18] D. Y. Kim, R. H. Scheicher, and R. Ahuja, Phys. Rev. B, **78**, 100102 (2008).
[19] I. Goncharenko, M. I. Eremets, M. Hanfland, J. S. Tse, *et al.*, Phys. Rev. Lett., **100**, 045504 (2008).
[20] P. B. Allen and B. Mitrovic, Solid State Physics, **37**, 1 (1982).
[21] W. L. McMillan, Phys. Rev., **167**, 331 (1968).
[22] P. B. Allen and R. C. Dynes, Phys. Rev. B, **12**, 905 (1975).
[23] P. B. Allen, Phys. Rev. B, **6**, 2577 (1972).
[24] G. D. Mahan, *Many-Particle Physics* (Klumer Academic, 2000).
[25] A. A. Maradudin and A. E. Fein, Phys. Rev., **128**, 2589 (1962).
[26] P. Giannozzi, S. Baroni, N. Bonini, M. Calandra, *et al.*, J. Phys. Condens. Matter, **21**, 395502 (2009).
[27] J. P. Perdew, K. Burke, and M. Ernzerhof, Phys. Rev. Lett., **78**, 1396 (1997).
[28] J. P. Perdew, K. Burke, and M. Ernzerhof, Phys. Rev. Lett., **77**, 3865 (1996).
[29] D. Vanderbilt, Phys. Rev. B, **41**, 7892 (1990).
[30] S. Baroni, S. de Gironcoli, A. Dal Corso, and P. Giannozzi, Rev. Mod. Phys., **73**, 515 (2001).
[31] To get a sense of scale, note that, for the ion most displaced, $|\mathbf{x}_{\kappa\nu_x}| \simeq 0.15\,a_0 \simeq 0.03\,a$ for X_1 and $|\mathbf{x}_{\kappa\nu_x}| \simeq 0.14\,a_0 \simeq 0.02\,a$ for X_2.
[32] T. Yildirim, O. Gülseren, J. W. Lynn, and B. *et al.*, Phys. Rev. Lett., **87**, 037001 (2001).
[33] M. Lazzeri, M. Calandra, and F. Mauri, Phys. Rev. B, **68**, 220509 (2003).
[34] M. d'Astuto, M. Calandra, S. Reich, A. Shukla, *et al.*, Phys. Rev. B, **75**, 174508 (2007).